A Novel Optical Sensor for Mirror Edge Sensing

D. A. H. Buckley[*a,b], F. Schindler[c], H. Gajjar[a,b], S. Leveque[d], J. W. Menzies[a,b] & K. Sändig[c]

[a]South African Astronomical Observatory, Observatory, Cape Town, South Africa
[b]Southern African Large Telescope, Observatory, Cape Town, South Africa
[c]Dr Johannes Heidenhain GmbH, Germany
[d]European Organisation for Astronomical Research in the Southern Hemisphere, Garching, Germany.

ABSTRACT

The Southern African Large Telescope (SALT) recently (2008) abandoned attempts at using capacitive mirror edge sensors, mainly due to poor performance at a relative humidity above ~60%, a not infrequent occurrence. Different technologies are now being explored for alternative sensors on SALT. In this paper we describe the design and development of a novel prototype optical edge sensor, based on the application of the interferential scanning principle, as used in optical encoders. These prototype sensors were subsequently tested at SAAO and ESO, for potential application on SALT and E-ELT.

Environmental tests, conducted in climatic control chambers, looked at temperature and relative humidity sensitivity, long term stability and sensor noise. The temperature sensitivity for height and gap were, respectively, 10nm/°C and 44nm/°C, while for relative humidity they were 4nm/10% and 50nm/10%, respectively. These either met, or were close to, the SALT specification. While there were significant lags in response, this was due to the sensor's relatively large mass (~200 gm per sensor half), which was not optimized. This is likely to improve, should a revised design be developed in future. Impressively the sensor noise was <0.015 nm RMS, over three orders of magnitude better than the specification. Our conclusions are that optical edge sensing is a viable technique for use on segmented mirror telescopes.

Keywords: large telescopes (SALT), segmented mirrors, mirror alignment, edge sensors, optical interferential sensing

1. INTRODUCTION

Mirror edge sensing is crucial in all segmented mirror telescopes for active control of the primary mirror segments. This technique was pioneered on the 10-m Keck I & II telescopes, for which the mirrors were phased in order to achieve the diffraction limit of the 10-m diameter mirror arrays. Each mirror segment needs to be controlled in both tip/tilt and piston, which is done by measuring relative mirror gaps and heights. A matrix inversion of the edge sensor measurements is then used to update mirror positions in space, using actuators, with 3 degrees of freedom (DOF) per segment.

For a full hexagonal array of m mirror segments with n rings (i.e. with no missing central segment), the total number of mirrors, m, is given by the expression:

$$m = 1 + \sum_{i=0}^{n} 6 \cdot i$$

The equivalent number of required edge sensor pairs, s, is then given by:

$$s = 6\,(m - (2n + 1)),$$

while the total number of degrees of freedom, which is also the total number of mirror tip, tilt & piston actuators, is:

$$p = 3\,m$$

[*] dibnob@saao.ac.za; SAAO, PO Box 9, Observatory 7935, South Africa; phone +27 21 4606286; fax +27 21 4473639;

In general two parameters are required to be measured by mirror edge sensors: gap and height (= piston). The latter is the most important measurement needed to assure that the mirrors are correctly aligned to the correct global shape. Gap, which is usually driven by temperature changes, normally only affects the global radius of curvature (GRoC, or so-called "focus mode").

For a series of edge sensor relative height measurements, $\boldsymbol{S}$ (an $s \times 1$ vector), then the resulting actuator response required to null the height changes is given as $\boldsymbol{P}$ (a $p \times 1$ vector), where $\boldsymbol{S} = \boldsymbol{A} \bullet \boldsymbol{P}$ and the matrix $\boldsymbol{A}$ describes the system geometry. From the edge sensor heights, the actuator responses are derived by inverting the last equation, namely $\boldsymbol{P} = (\boldsymbol{A}^T\boldsymbol{A})^{-1}\,\boldsymbol{A}^T \bullet \boldsymbol{S}$ (see, e.g. [1]).

In general, the mirror support system (including the individual mirror mounts and the supporting truss) dimensions change slowly with time, being driven by temperature and gravity changes. The mirrors themselves are much less prone to dimensional distortions due to: 1.) a lower coefficient of thermal expansion (CTE) compared to the typical steel supporting system (orders of magnitude less CTE if a typical low expansion glass ceramic is used), and 2.) mounts that support the mirrors without distorting them as they change dimensionally. The gradual thermal misalignments of the mirror segments can occur over timescales of minutes to hours, depending on the temperature changes. Gravity changes, if they occur (as in the Keck telescopes), happen continuously and typically at a shorter timescale compared to thermal variations as the telescope mirror changes orientation.

Precise mirror edge sensing, used to correct for primary mirror misalignments, was pioneered on the Keck I & II telescopes using capacitive edge sensors mounted on the mirror backs. Gap, height and dihedral angle (relative tilting of mirror segments) are able to be measured by these sensors. In addition, the optical alignment of the segments is done with a phasing camera, in combination with the mirror actuators, which can position and sense the mirror heights such that the relative pistoning of neighboring mirror segments is known to an accuracy of $n\lambda/4$. This is referred to as being "phased" and is required if the diffraction limit of the entire 10-m diameter ensemble of mirrors is to be achieved. The resolution of the edge sensing is therefore critical to maintain alignment of the mirrors, and typically requires measurements with an accuracy of < 20 nm.

The second generation of segmented mirror telescopes, namely the Hobby-Eberly Telescope (HET; completed in 1997) and the Southern African Large Telescope (SALT; completed in 2005), designed to be seeing limited telescopes, had less stringent requirements in terms of pistoning (10 – 15μm RMS), without phasing the primary mirror. Even so, mirror tip/tilts still need to be well controlled (e.g. to ± < 0.1 arcsec) in order not to degrade the image quality. HET initially planned not to use edge sensing and proposed instead to adopt a thermal FEA model, together with many active temperature measurements throughput the mirror truss. This procedure never really succeeded, which led SALT to adopt edge sensors from the beginning of the project, as did eventually the HET. Of the 6 existing segmented mirror telescopes, 4 use capacitive edge sensors (Keck I & II, SALT (initially), and GTC) and 2 use inductive or eddy current sensors (HET and LAMOST).

2. SALT CAPACITIVE EDGE SENSOR EXPERIENCE

The 10-m Southern African Large Telescope (SALT)[2] is based on the "optical Arecibo" design, pioneered by HET, and has a fixed elevation of 43º. Unlike the Keck telescopes, the active optics control for SALT only has to deal with temperature driven misalignments. The construction phase of SALT and its first two "first-light" instruments[3] was completed in November 2005, which was followed by a period of commissioning, performance verification and early science[4], which extended through to April 2009. The SALT primary mirror (M1) array consists of 91 segments, each 1.2-m corner to corner and 50 mm thick, with a spherical figure of 26.165 m radius of curvature. Unlike the Keck telescopes, and like HET, the SALT M1 mirror segments are not phased, since SALT is a seeing limited telescope. Therefore the piston accuracy for the M1 array is a relaxed 15 μm RMS, which is currently achieved using a spherometer, and maintains piston for ~months at a time. The tip/tilt alignment of the segments is achieved using a Shack-Hartmann wavefront sensor, situated at the centre of curvature in an alignment tower[5], which routinely aligns the M1 array to ~0.06 arcsec RMS in good conditions (low wind).

The initial SALT segment alignment and maintenance system (SAMS-I) was based on capacitive edge sensors consisting of thin Cu strips with a conformal coating glued onto the edges of each of the mirror segments[6],[7]. All 91 hexagonal mirrors had nominally identical sensors on each of the 6 sides, giving a total of 546 sensor pairs, consisting of of opposing transmitter and receiver plates, although only 480 were used to make measurements at a given time due to the

inactive sensors on the outer edge of the 5th ring of segments. These outer segments still required the edge sensors to be attached in order to allow them to be moved anywhere in the primary mirror array, which can occur when segments are re-coated. This is unlike the case for the Keck telescopes, which have segments with paraboloid, rather than spherical, surfaces. The SALT segment positioning system (SPS) consists of 273 actuators, i.e. 3 per mirror segment.

The control algorithm for the mirror segments was based on solving the matrix inversion, as discussed in Section 1, with the requirement to control mirror tip/tilts to < 0.1 arcsec rms. This is required to achieve the image quality error budget for the primary mirror array of < 0.44 arcsec EE50 diameter. In addition, the system is specified to hold alignment, with < 10% degradation, over a *continuous* period of 5 days/nights. The control loop also had to account for noise (sensor & actuator), gain, etc., and the final implemented control flow diagram is shown in Figure 1.

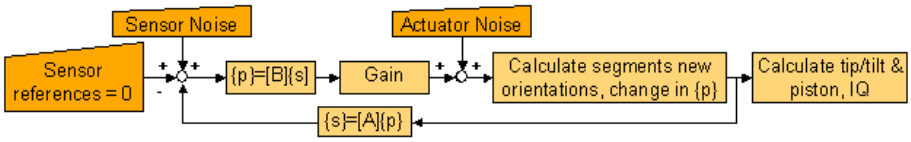

Figure 1: The SALT SAMS control flow diagram.

Following protracted tests both on and off the telescope, the original capacitive sensors were found to be inadequate for the task, primarily owing to their intrinsic sensitivity to relative humidity (R.H), which tends to vary significantly at Sutherland (the diurnal change in R.H. exceeds 50% for 40% of the time). In addition, the acceptance testing of the edge sensors revealed non-repeatable sensor behaviour and sensor noise levels that were both variable and dependent on temperature and R.H. Marginal success was only obtained on sub-arrays (1 – 3 rings) of the primary mirror and really only controlled the mirror well in stable conditions (low R.H and or ΔTemp), when edge sensors were hardly needed.

The most likely reasons for the capacitive sensors not meeting the SALT specifications are micro-condensation on the surface of the sensor, leading to moisture absorption by the sensor components. The effect is exaggerated by the relatively larger mirror gap sizes, namely a range of 6 – 22 mm. In addition, the R.H. and temperature dependencies are affected by the presence of dust particles on the sensor plates. In early 2008 we declared the SAMS-I capacitive system a failure and have since been pursuing a program to identify alternative technologies for mirror edge sensing. This work has paralleled investigations by other groups building segmented mirror telescopes, namely LAMOST, TMT and E-ELT. As part of this program we have been involved in the development and testing of *inductive* edge sensors, from 3 manufacturers and an optical interferential edge sensor, which is the subject of the current paper.

3. THE DEVELOPMENT AND PRINCIPLE OF OPTICAL EDGE SENSING

Since 2007, the company Dr Johannes Heidenhain GmbH has been involved in an R&D development program for optical edge sensors as part of an E-ELT design study for ESO. Since 2008 (after contacts made at the Marseilles SPIE meeting) SALT became involved in a co-operative program with Heidenhain for the development of potential prototype optical edge sensors. The aim was to assess the performance of such a prototype with a view to demonstrating viability for a full new (SAMS-II) system.

The Heidenhain-ESO collaboration culminated in the development of a “proof of concept” optical sensor, referred to as the Mk I sensor. The design and operation of this Mk I prototype is based on the well-recognized and developed optical encoding technology pioneered by Heidenhain. The MkI sensor has been tested by ESO and two prototypes were also sent to SALT in Oct 2008 for in-house testing in climatic chambers. Regrettably one of those sensors was damaged in transit, which meant that only one such sensor could be tested at SALT.

The Mk I prototype uses the interferential scanning principle as used in Heidenhain optical encoders. A “scale” is engraved with chromium on a Zerodur plate with a pitch of 2 microns. This is positioned behind a semi-transparent reticle structure with the same pitch. The reticle is illuminated with collimated light from a diode source which splits the beam into 3 parts: the zero order and the +1 and – 1 diffracted spectral orders. These are reflected by the scale and sent back to 3 photocells which detect the – 1, 0 and +1 spectral orders. Measuring the phase shifts between the 3 signals gives the relative displacement of the scale and reticle, with a typical resolution determined by pitch divided by 2048 or even 4096 (i.e. < 1 nm). In Figure 2 we show the basic principle of the method.

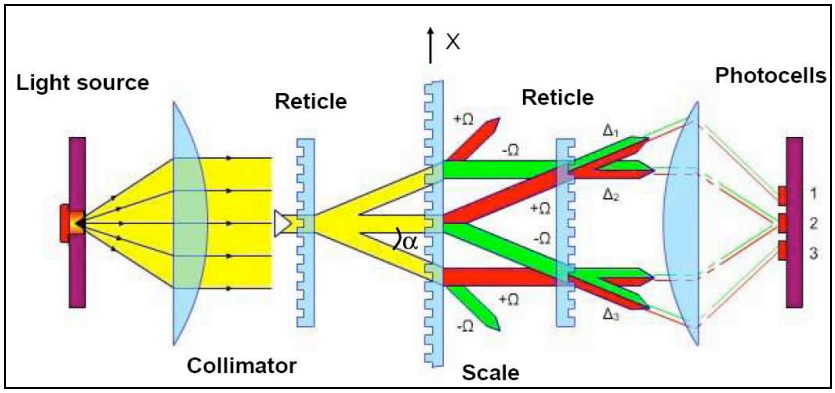

Figure 2: The operational principle of interferential scanning as used in optical encoding and the basic principle of the Mk I sensor.

The schematic shown in Figure 2 demonstrates how the light is dispersed by the semi-transparent reticle and the reflective scale and how the spectral orders recombine. The scale is in the centre of the diagram, which moves relative to the reticle (in X), while the transmissive reticle is shown both to its left and right, showing the incident and diffracted beams before and after being reflected/diffracted by the scale. While two reticles are shown, in reality there is just one, but light passes through it in both directions. This is shown more clearly in Figure 3 below.

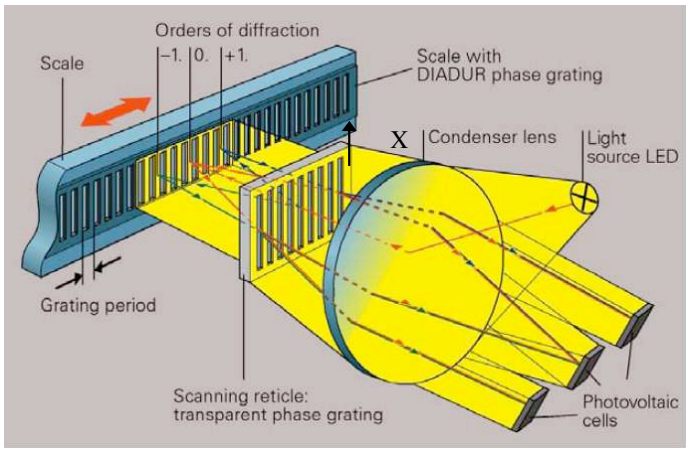

Figure 3: Schematic of the optical layout of the interferential optical sensing system as used in the Mk I optical edge sensor.

Light falling on the reticle is transmitted and orders $n = -1$ and $+1$ are diffracted by the reticle at an angle α given by the grating equation, $\sin\alpha = \lambda / C$, where C is the pitch of the reticle ruling (= 2 μm, i.e. d = 500 lines/mm), with roughly equal intensities with the un-diffracted ($n = 0$) component. These orders are then diffracted by the scale, mostly into orders $n = -1$ and $+1$, which imposes a phase change of $\Omega = 2\pi X/C$ depending on the scale's relative movement, X, with respect to the reticle. These partial waves meet again at the phase grating of the scanning reticle where they are diffracted again and interfere. The interference between the recombined orders leads to an intensity modulation of the resulting signal at a frequency of twice that of the scale ruling. There are essentially 3 wave trains that leave the scanning reticle at different angles and are detected by 3 photovoltaic cells. A resulting phase shift of ±120° occurs between the different interference paths. The zero order from the reticle is also dispersed by the rule, and these diffracted orders also interfere with the two diffracted orders from the reticle. This zero order interference leads to the determination of an absolute position (index signal), while the -1 and $+1$ order interference phases changes just provides the relative movement between the reticle and the scale. In Figure 4 we show schematically how the phases changes occur for the three interfering signals (from $n = -1, 0$ and $+1$) detected by the three photocells shown in Figure 3.

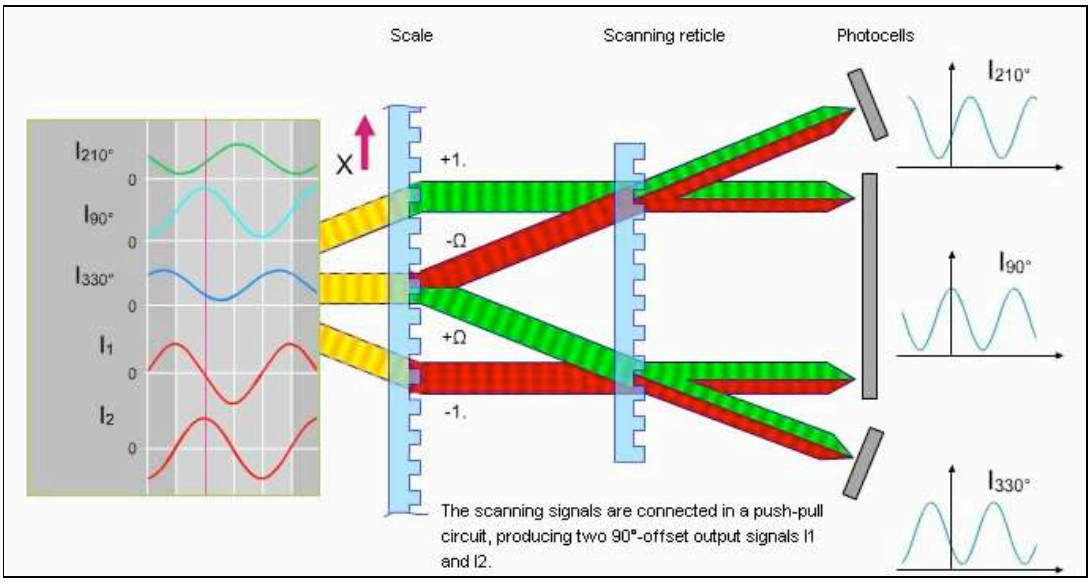

Figure 4: Phase changes between the three interference orders (– 1, 0 +1) produce a modulated intensity variation, detected as a voltage variation from the three photovoltaic cells.

Relative motions of the reticle and scale causes the two diffracted wavefronts to undergo phase shifts of ± Ω. When the relative motion is one grating period (C), then the wavefront of the n = +1 order is displaced by one wavelength in the positive direction ($\Omega = 2\pi$), while for the n = – 1 order, the wavefront is displaced by one wavelength in the negative direction (($\Omega = -2\pi$). Phase shifts of fractions of a wavelength produce relative phase shifts of the signals, which cause the detected signals to vary. This varying signal is used to compute the phase shifts, and hence the relative motions of the reticle and scale. By choosing a suitable geometry, two sensors can in principle measure motions in two orthogonal directions, which in this case is piston and gap.

4. THE PROTOTYPE MK I SENSOR

The Mk I optical edge sensor consists of thee pairs of opposing reticles and rules, each mounted on a "stylus" which is bonded magnetically to buttons glued to the backs of mirrors. One stylus has the light source, the three reticles and the three photocell detectors, while the stylus on the neighbouring segment has three matching scales. Two of the reticle – scale pairs are tilted by ±100 mrad (~6º) to the piston direction (z). Piston (Δz = height) and gap (Δy) changes between the segments result in relative motion between the reticles and scales, which are detected from the intensity changes measured by the two respective photocells. A third sensor measures the interference with the zero order from the reticle, and provides an absolute position reference, which is used when the system is rebooted.

In Figure 5 we show a schematic of the Mk I sensor, which shows the orientation of the two reticle–scale pairs comprising the two optical displacement sensors which are used to measure the relative piston and gap changes between mirror segments. The vectors X1 and X2 shows the sensing direction for the two displacement sensors, which are rotated with respect to the piston (z) direction by θ = ±100 mrad. Motion in either piston or gap will produce motion in the X1 and X2 directions, which are sensed and averaged. The X1 and X2 motions are then easily deconvolved into the respective gap (Δy) and piston (Δz) motions using the following formulae:

$$\text{Piston } (\Delta z) = (X1 + X2) / 2 \cos\theta = (X1 + X2) \times 0.5025 \qquad \text{[Eq. 1]}$$

$$\text{Gap } (\Delta y) = (X1 - X2) / 2 \sin\theta = (X1 - X2) \times 5.0083 \qquad \text{[Eq. 2]}$$

In practice the reticles and scales are not perfectly aligned with each other, due to installation tolerances. This implies that there is a relative angular offset between the two, which is typically of order ~1 mrad (~0.1°), which results in parasitic motion detection (i.e. apparent motion detected which is not real, being a consequence of the mounting tolerance).

In Figure 5 we show a schematic of the Mk I optical sensor, with the two reticle–scale pairs, inclined to the vertical piston direction, used to measure gap and piston. The absolute indexing is achieved with an additional displacement sensor, not shown.

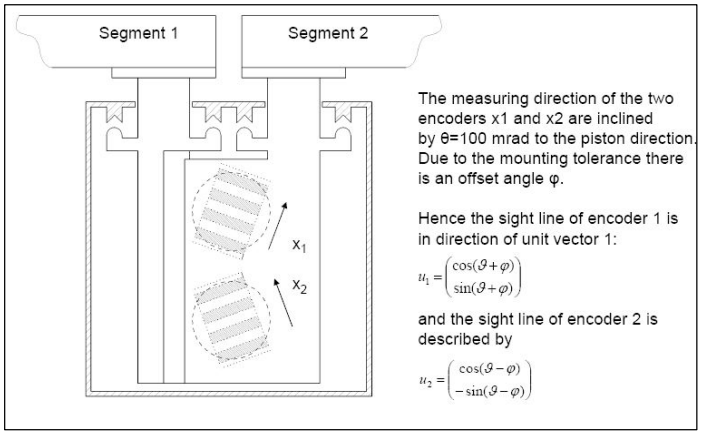

Figure 5: Schematic of the Heidenhain Mk I optical edge sensor. Two reticle–scale pairs measure motion in two different directions, namely X1 and X2, which can then be deconvolved into gap and piston measurement. The relative angular offsets of the reticle–scale pairs are dictated by the more demanding requirement for piston (z) sensitivity. A "stylus" is attached to each segment, one containing the reticle and the other the matching scale.

Because the sensor is required to be light-tight, the two styli are enclosed in a sealed box with a rubber bellows between them and the enclosure. To avoid placing too much weight on the mirror segment, this box is independently supported by a connection to the supporting mirror truss. While this is an undesirable added complication, which would preclude use in a real telescope, it was sufficient for the purposes of a conceptual proof of concept. A photograph of a Mk I sensor, with a square hole cut in the cover to allow viewing of the internal components, is shown in Figure 6.

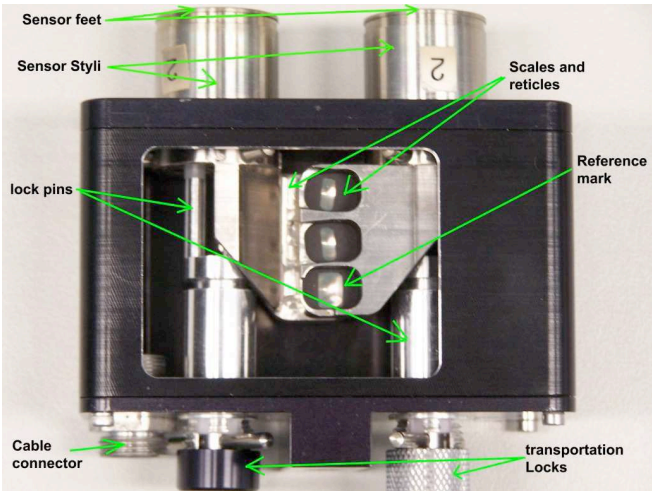

Figure 6: A photo of the Heidenhain Mk I optical edge sensor showing the various components. The light source and photodiodes are hidden behind the metal housing for the three scales.

A schematic of the sensor, identifying the various components, is shown in Figure 7.

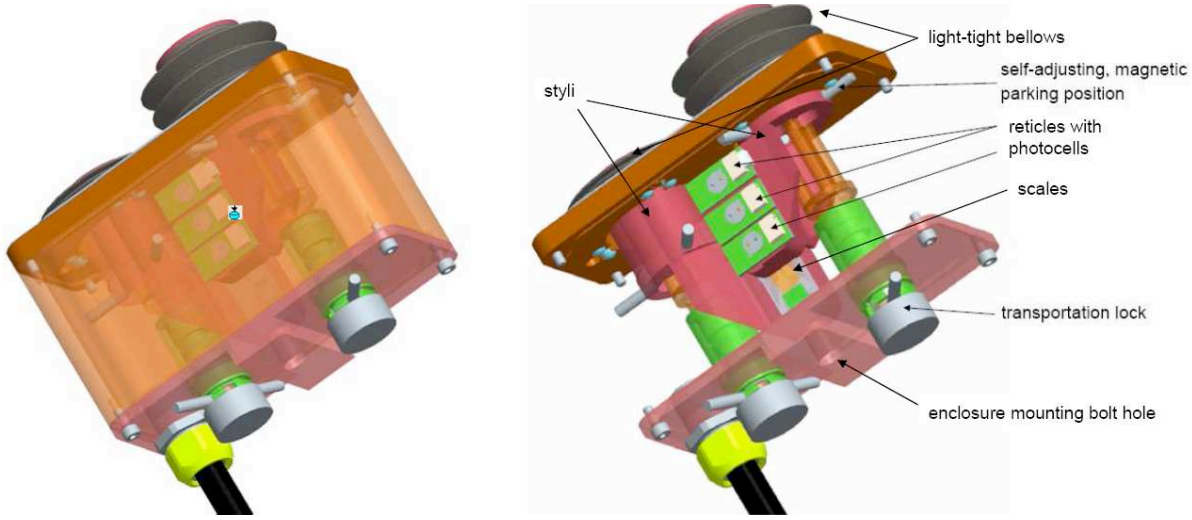

Figure 7: Schematic of the Heidenhain MkI optical sensor identifying all of the major components. The semi-transparent box shown at the right is the sealed enclosure of the sensor. The styli are free to move with respect to this box, and have a rubber bellows to avoid light leaks.

A scheme for mounting the Mk I sensors on a mirror array is shown in Figure 8, although subsequent requirements concerning maximum allowable mass (to avoid distorting the mirror figure), has ruled out mounting these sensors in such a manner (they weight ~ 400 gm). The enclosure box has a mounting bolt hole at the rear which could be used to mount the box independently to the primary mirror truss, although this was ruled out for SALT and E-ELT.

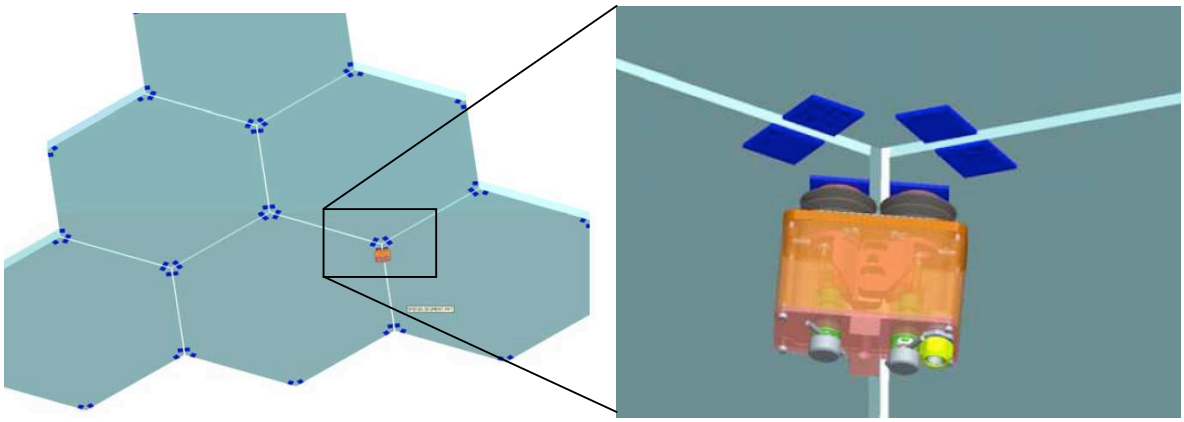

Figure 8: A possible mounting configuration for the Mk I sensor on the back of a mirror array.

5. PERFORMANCE TESTING OF THE MK I SENSOR

In this section we describe the testing methodology for the Mk I sensor carried out by us at Heidenhain, ESO and SALT. These tests were designed primarily to investigate the effects of both temperature (T) and relative humidity (R.H.) on the sensor's performance. A special Invar test stand was manufactured by Heidenhain which was designed to hold two sensors, allowing independent tests. This stand could then be mounted in climatic test chambers, which allow us to control, independently, both T and R.H. The stand could also be rotated to simulate gravity changes (not relevant for the SALT tests).

The tests conducted at ESO also involved an alternative testing rig, which in principle could make independent piston/gap measurements with an interferometer, while simultaneously testing the performance of both the Mk I optical sensor and alternative prototype inductive sensors. Similar sets of tests were also completed at SALT, but without the benefit of interferometers. As it turned out, unfortunately the interferometers used in the ESO tests were incapable of independently measuring piston and gap at the precision required, due primarily to thermal sensitivity drifts. In Figure 9 we show the test set up at ESO, which was designed to investigate performance of both the Mk I sensors (for piston and gap) and an alternative inductive sensors from Fogale Nanotech (for piston, gap and shear). Dynamic shear is an issue for E-ELT, as segments are expected to move in shear as the orientation of the telescope changes. For SALT, with its fixed altitude, this is not an issue, although static shear is (i.e. segment offsets in the x (shear) – y (gap) plane from their ideal position). In addition ESO conducted tests on susceptibility to RF interference.

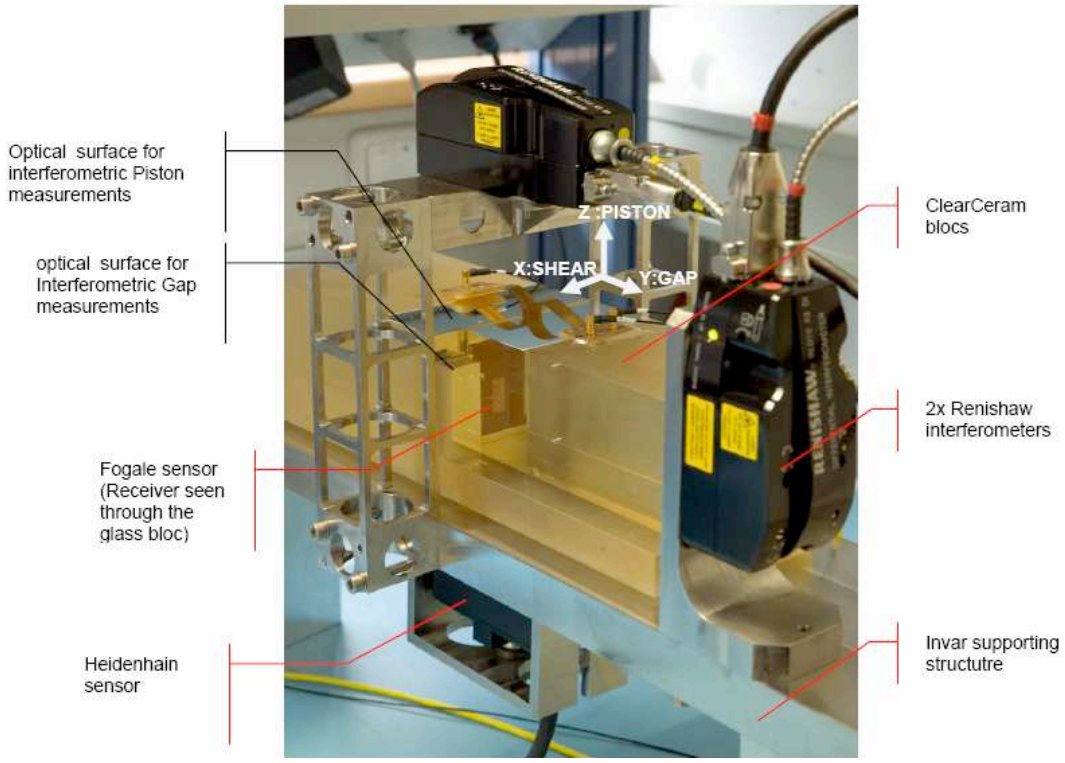

Figure 9: The test setup at ESO used to investigate the performance of various types of edge sensor prototypes. The Mk I sensor is seen at the bottom.

The tests conducted at SALT were only done on a single Mk I sensor, rather than two, as unfortunately the second sensor was damaged in transit. In Figure 10 we show the sensor mounted in the Invar test stand, plus the associated power supply and first stage of the signal processing electronics.

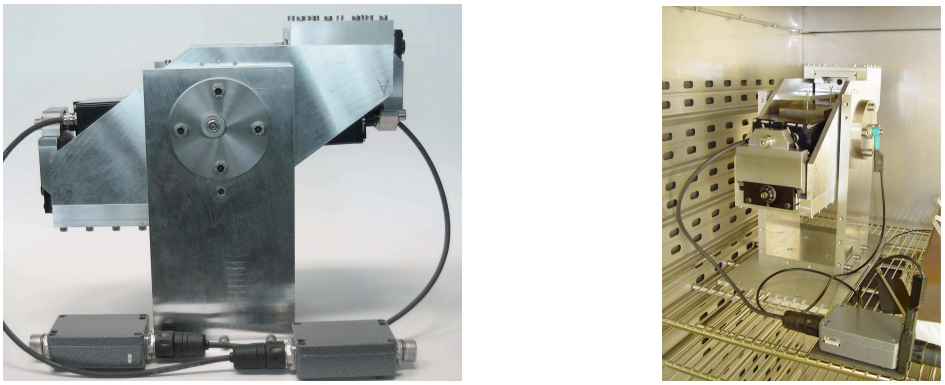

Figure 10: The Invar test stand, with two Mk I sensors mounted (left) and inside the SALT climatic test chamber (right).

The testing consisted of cycling either T (at constant R.H.) or R.H (at constant T) over time and measuring the response of the sensor in terms of its piston and gap measurement. The ESO tests had the styli mounted on two different ClearCeram (low CTE glass-ceramic) blocks, for which relative gap and piston could be adjusted. In contrast the Invar test stand used for the Heidenhain and SALT tests had the styli connected to single Invar block.

The main aim of the tests was determine the intrinsic sensitivity of the Mk I sensor to both T and R.H. Any changes in the measured piston or gap by the sensor would be due to such sensitivity, since the low CTE test pieces (made of ClearCeram and Invar) should not produce any real dimensional change with temperature (although in fact the higher CTE of Invar could, in principle, lead to a perceived gap change as the single Invar block expands and contracts).

6. HEIDENHAIN TEST RESULTS

Here we present the results of the tests conducted on the Mk I sensor as described in the previous section. We show the Heidenhain results in Figure 11. For the temperature tests (Fig. 11; left), the sensor was subjected to a variation of T = 13 – 23ºC, which resulted in a piston variation of Δz = 50nm, at 4 nm/ ºC. This was within the SALT specification of < 7nm/ ºC. The R.H. tests (Fig. 11; right) varied relative humidity from 30% – 80% (for T = 25 ºC), resulting in a gap variation of 120nm (PtV) and piston variation of 20 nm (PtV). The latter implied a piston sensitivity of 0.4 nm/R.H.%, compared to the SALT specification of < 0.5 nm/R.H.%.

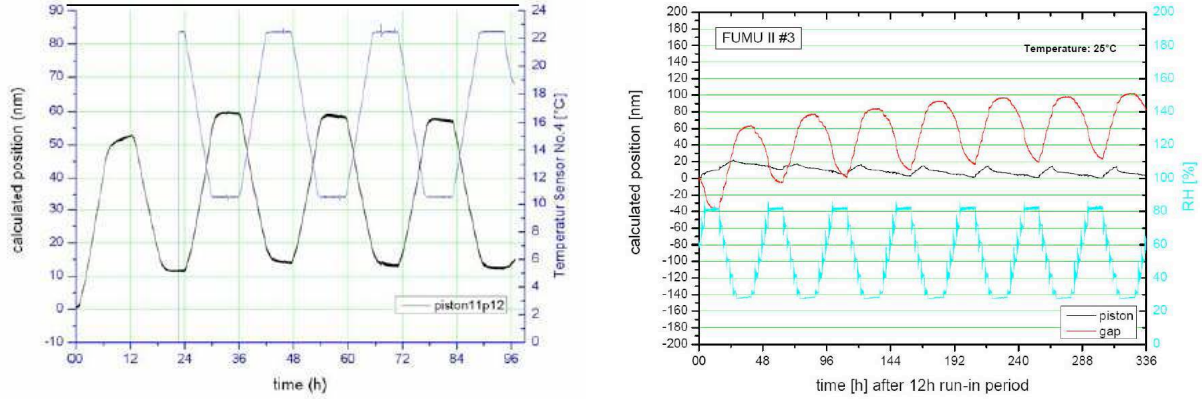

Figure 11: Heidenhain test results for the Mk I optical sensor for (left) temperature variations (T = 13 - 23ºC) and (right) relative humidity variations (R.H. = 30 – 80%).

Sensor noise tests showed that the Mk I sensor had an extremely low piston measurement noise level of <0.5 nm for 2kHz measurement sampling, less than the quantization step.

7. ESO TEST RESULTS

Some of the test results conducted at ESO are shown in Figure 12, which shows (left) the long term drift of the piston over a ~15 day test period. For this test the sensor was inside the climatic chamber, which was not controlled, while the sensor electronics were at ambient conditions in the laboratory. For the duration of the test, the chamber temperature varied by 1ºC (PtV), while the electronics varied by 3ºC (PtV). The total piston variation was ~30nm and correlates to both diurnal and longer timescale variations in ambient temperature. Part of the piston signal is due to the residual mechanical fluctuations of the test bench, and are not necessarily intrinsic to the sensor. One problem encountered in these tests was interference produced by the climatic chamber fans. For this reason the fans were turned off for the RH tests once the desired set point was reached.

For the test shown in Figure 12, right, the climatic chamber was first set to R.H. = 5%. After this had been reached the control of the chamber was switched off (i.e. no vibrating fans) with the piston and temperature recorded for ~60 mins. Then the chamber was reset to R.H. = 95%, during which the fans were running, and again once the new set point was reached, the fans were switched off while data was recorded, again for ~60 min. The results from these tests showed a R.H. sensitivity of ~0.3 nm/RH%. Noise tests confirmed the low values obtained by Heidenhain, as shown in Figure 13. EMC tests of RF interference showed no effects over a 80 – 1000 MHz bandwidth for emission levels of up to 3V/m.

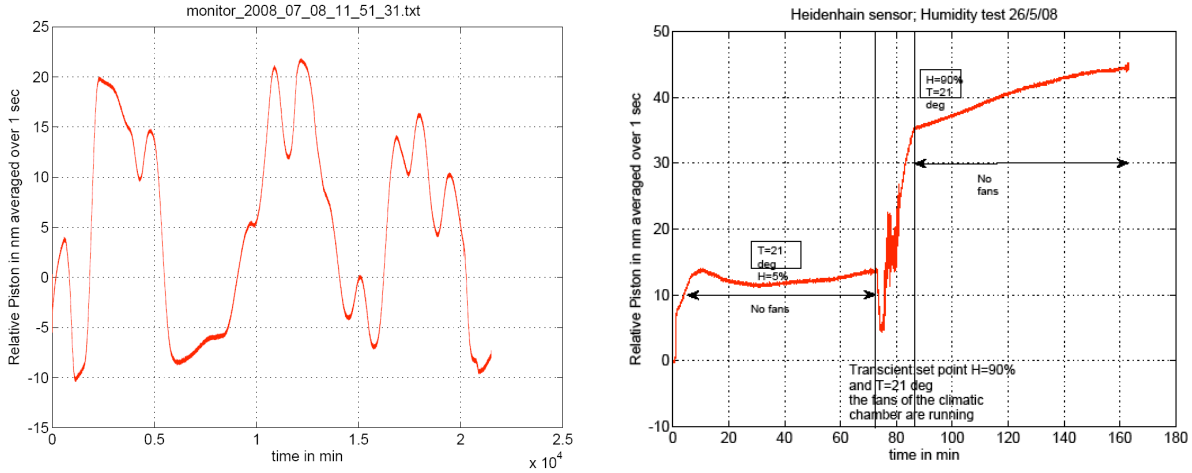

Figure 12: ESO Mk I sensor tests (see text). Left: long-term (~15 day) ambient test. Right: R.H tests at R.H. = 5% (first half) and 95% (second half) for a constant T = 21ºC. The increasing piston in the second half of the test is correlated with a linearly increasing temperature (ΔT ~ 0.5º).

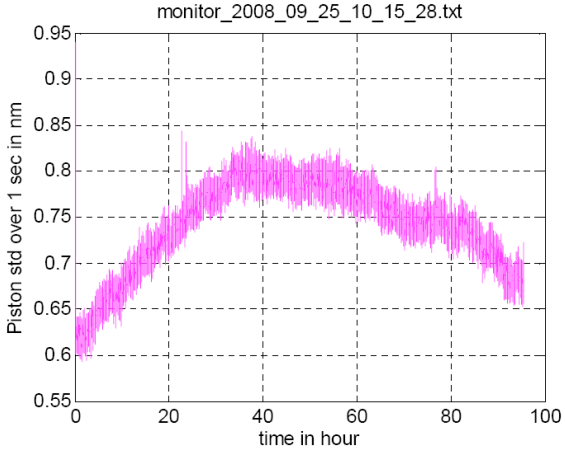

Figure 13: ESO noise measurements (piston standard deviation in nm) of the Mk I sensor measured over 95 hours.

8. SALT RESULTS

A similar series of repeated tests, as described above, were carried out at SALT on one of the Mk I sensors, mounted to the Invar test stand. Both temperature and relative humidity sensitivity tests were successfully conducted, without the problems of interference from the climatic chamber circulation fans which affected the ESO results. In Figure 14 we show an example of a temperature test and in Figure 15 a similar test for relative humidity.

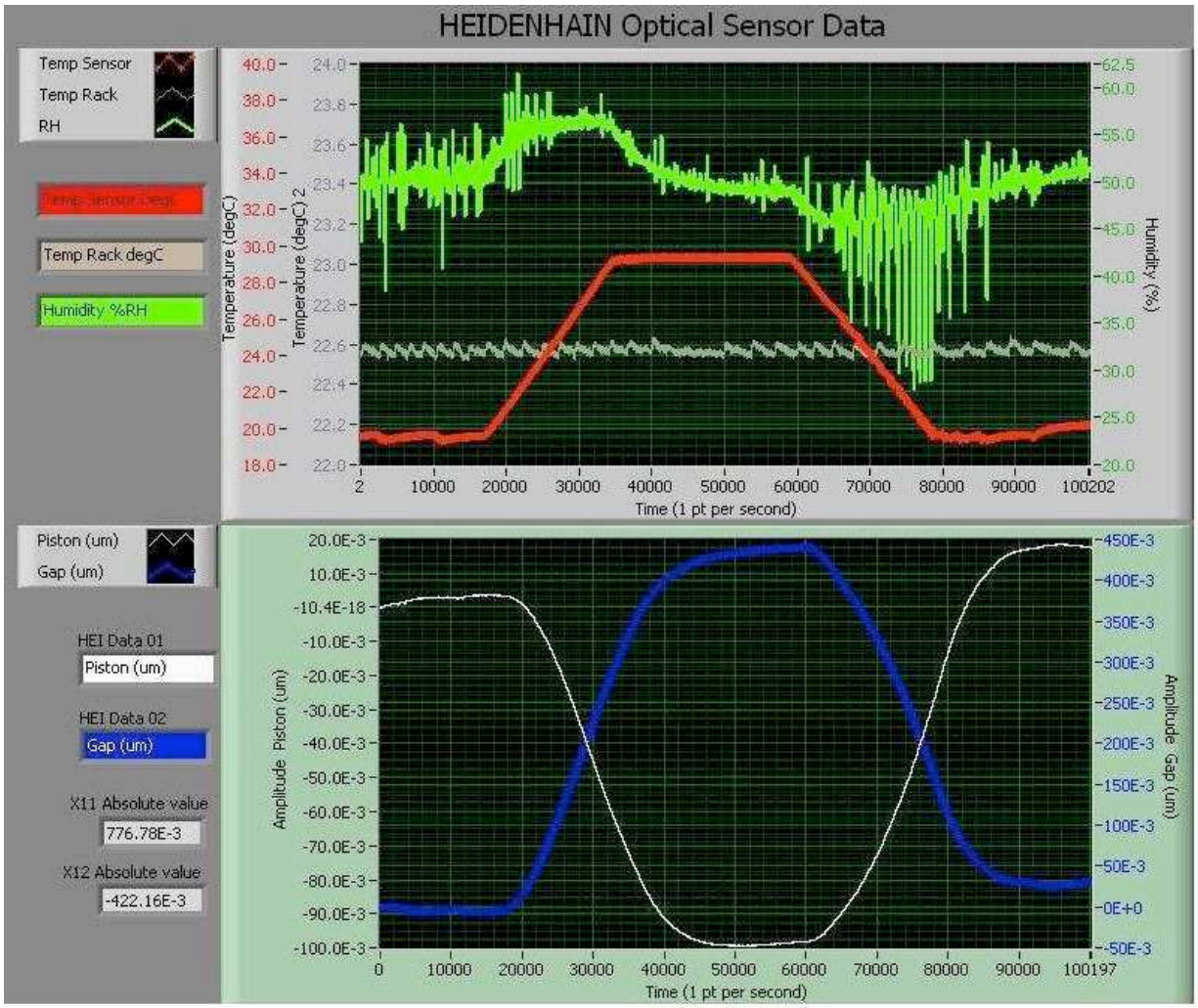

Figure 14: SALT temperature sensitivity test run of ~28 hours for the Mk I sensor. Top: the environmental conditions are graphed, showing the ramping temperature from T = 20 – 29 ºC (red; first left *y*-scale), constant R.H. ~ 50% (green; right *y*-scale), and temperature of the electronics cabinet T = 22.6 ºC (grey; second left y-scale). Bottom: the variation in piston (white; left *y*-scale) and gap (blue; right *y*-scale).

Results from repeated testing at SALT show that the Mk I sensor drifts in piston and gap by 10nm/°C and 44nm/°C, respectively, with some observable lag in response. These values are somewhat higher than the ESO measurements, but it is possible that there will be variations between sensors. Most of this drift is probably attributed to the prodigious use of metal used in the construction of the sensor and test stand.

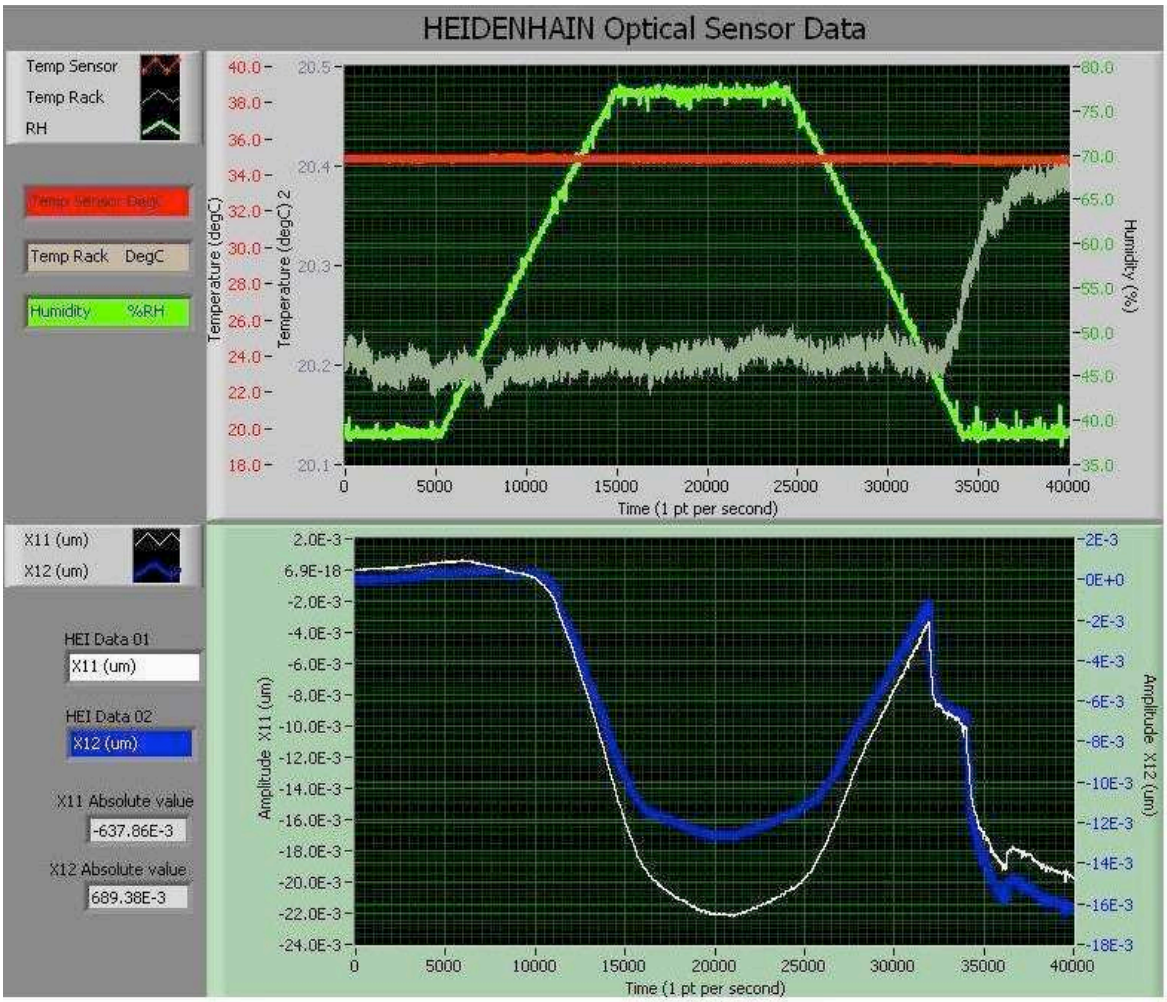

Figure 15: SALT relative humidity sensitivity test run of ~11 hours for the Mk I sensor. Top: the environmental conditions are graphed, showing the ramping R.H. from 38% to 78% (green; right *y*-scale), constant T = 35 ºC (red; first left *y*-scale), and temperature of the electronics cabinet T ~20 ºC (grey; second left y-scale). Bottom: the variation in X1 (white; left *y*-scale) and X2 (blue; right *y*-scale), which are used in equations [1] and [2] to calculate piston and gap (see Section 4) .

The R.H. results from these tests indicate a response of the sensor of 0.4 nm/R.H.% and 5 nm/R.H.%, respectively, for piston and gap, which is within the SALT specifications. Noise measurements for the sensor indicate a staggeringly low level of 0.005 nm and 0.015 nm RMS, respectively, for piston and gap.

9. CONCLUSIONS

The performance testing we have undertaken of the Heidenhain Mk I optical sensor indicates that it meets the fundamental metrological requirement of detecting dimensional changes at the nanometer level, required for measuring relative piston and gap motions of mirror segments, while at the same time being sufficiently insensitive to environmental changes (temperature and relative humidity). There are, however, several issues that would need to be addressed before such a sensor could be realistically deployed as an edge sensor on a segmented mirror telescope. These are now discussed.

Firstly, the sensor suffers from a high thermal time constant, often only responding after ~1 to 4 hours to any change in either temperature or relative humidity. This is most likely due to the large amount of metal, with consequent thermal inertia, used in the Mk I sensor. Any revised design (see next section) should use less metal in its construction to have a correspondingly lower thermal mass.

One other major issue is that the Mk I sensor is not able to function correctly with a dihedral angle greater than ~0.05º (~1 mrad), whereas the static taper angle between adjacent SALT segments is 2.2º. Few things can be done to address this at the sensors level, except increasing the scale pitch, which is undesirable because of the loss of resolution. However, this static taper angle could probably be taken into account in the design (e.g. of the styli and their mounting), allowing the scale to be tilted by 2.2º. More worrisome is the *dynamic* range of the taper angle experienced by typical segment misalignments, which can vary by as much as ± 0.1º from the static value. This exceeds the current Mk I sensor's capture range by a factor of ~2×.

In addition, a special mounting scheme has to be developed to cope with the range of static mirror gaps (6 – 22 mm) and static shears (up to 7 mm). An initial concept to address this involves mounting of a pivot contact point (ball in a cage or magnetic concave surface on convexes) between the mounting pad on the segment and the sensor styli.

10. FUTURE DEVELOPMENTS

While we have shown that the MkI sensor is capable as performing as an edge sensor in a laboratory test, we have identified several issues that currently preclude its use in a real telescope system. The major issue is the bulk of the sensor, which is too massive (~400 gm) and consequently with too high a thermal time constant. Because of the distorting effects of the sensor on the mirror figure, the Mk I prototype could only work if the enclosure box (i.e. the "chassis") was independently mounted to the truss in some manner. This was ruled out by ESO and SALT and led Heidenhain to conceptualize a "second generation" (i.e. Mk II) prototype design, which is shown in Figure 16.

The main principle of the Mk II design is for each half of the sensor to be mounted to adjacent segments and linked by a light-tight and dust-tight rubber bellows. The advantages of this concept are:

- Avoids using a 3rd contact point for the enclosure box
- Reduces the total height of the sensors by removing the transportation lock
- Reduces the metal part of the sensors, that will reduce the total weight and thermal lag of the sensor
- Would account for the range in gap (6 – 22 mm) and shear (< 7mm), depending on the mounting point.

A possible disadvantage of such a design is that it would require a more complex, adjustable, mounting scheme, which would also necessitate a complicated set-up calibration.

Figure 16: Conceptual design of the Mk II Heidenhain optical sensor. The two halves contain, respectively the reticle and scale and are mounted to adjacent mirror segments. A light-tight bellows would surround the gap between the two halves.

11. CONCLUDING REMARKS

In this paper we have amply demonstrated the potential viability of optical metrological sensing techniques, as routinely used in optical encoding technology, as edge sensors in segmented mirror telescopes. The company Dr Johannes Heidenhain GmbH , in collaboration with ESO and SALT, have developed a Mk I sensor as a proof of concept for such an edge sensor. Through independent testing by Heidenhain, ESO and SALT, this sensor has been shown to have both sufficient resolution, repeatability and insensitivity to the environment (temperature and relative humidity) to meet the basic requirements for both piston (height = Δz) and gap (Δy) determination.

The low intrinsic sensitivity of the sensor to both T and R.H. and the low noise level of the sensor is very encouraging. However, before such a sensor could be routinely employed as a telescope mirror edge sensor, there are several issues that will need to be addressed. Primarily this involves decreasing the mass of the sensor such that it will not affect mirror surface figure, through distortion, and will have a shorter thermal time constant to improve its response time.

We believe that the development of a Mk II version of this sensor, which would address these issues, is both technically viable and desirable. In 2008 Dr Johannes Heidenhain GmbH were indeed planning such a development, but the advent of the global financial crisis has regrettably stopped this development for now. However, our hope is that someday this technology will be further exploited.

ACKNOWLEDGMENTS

DB, HG & JWM would like to acknowledge the many people who have helped in developing SALT over the years, including the Project, Instrument and Operations Teams, the staff of the South African Astronomical Observatory, the many people at the various institutions in the SALT consortia, and those external to SALT who have lent support and assistance over the years.

REFERENCES

[1] Gajjar, H. et al., *Proc SPIE* **6267**, 626737, (2004).
[2] Buckley, D.A.H., Swart, G. P. and Meiring, J.G., *Proc. SPIE* **6267**, 62670Z (2006).
[3] Buckley, D.A.H., et al., *Proc. SPIE* **7014,** 701407, (2008).
[4] O'Donoghue, D., et al., *MNRAS* **372**, 151-162 (2006).
[5] Wirth, A., Gonsiorowski, T., Roberts, J., Bruno, T., Swiegers, J., Gajjar, H. and Swat, A.,*Proc. SPIE* **5489**-120, (2004).
[6] J. Swiegers, H. Gajjar, D. Roziere, A. Courteville, S. Buous, *Proc. SPIE* **5489**-149, (2004).
[7] J. Swiegers and H. Gajjar, *Proc SPIE* **5489**, 881-891 (2004).